Research Paper
J. Astron. Space Sci. 33(3), 167-172 (2016)
http://dx.doi.org/10.5140/JASS.2016.33.3.167

JASS Journal of Astronomy and Space Sciences

Recent *H*-alpha Results on Pulsar B2224+65's Bow-Shock Nebula, the "Guitar"

Timothy Dolch[1,2†], Shami Chatterjee[2], Dan P. Clemens[3], James M. Cordes[2], Lauren R. Cashmen[3], Brian W. Taylor[3]

[1]Hillsdale College, Hillsdale, MI 49242, USA
[2]Cornell University, Ithaca, NY 14850, USA
[3]Boston University, Boston, MA 02215, USA

We used the 4 m Discovery Channel Telescope (DCT) at Lowell observatory in 2014 to observe the Guitar Nebula, an *Hα* bow-shock nebula around the high-velocity radio pulsar B2224+65. Since the nebula's discovery in 1992, the structure of the bow-shock has undergone significant dynamical changes. We have observed the limb structure, targeting the "body" and "neck" of the guitar. Comparing the DCT observations to 1995 observations with the Palomar 200-inch Hale telescope, we found changes in both spatial structure and surface brightness in the tip, head, and body of the nebula.

Keywords: interstellar medium, pulsars, shock waves, neutron stars

1. INTRODUCTION

Many pulsars throughout the Galaxy have high spindown energy outflows and/or high velocities. Under favorable conditions, they are accompanied by bow-shock pulsar wind nebulae with radio, optical, and/or X-ray structure. Recent bow-shock nebula search campaigns targeting *Fermi*-LAT have discovered pulsars (Romani et al. 2010; Brownsberger & Romani 2014) and have brought the list of currently known *Hα* bow-shock nebulae to nine. Bow-shock nebulae frequently occur around canonical (non-millisecond) pulsars, which are more likely to have high $\dot{E}$ values due to their young ages (where $\dot{E}$ is the spindown luminosity in erg/s), as well as high velocities compared to millisecond pulsars (MSPs). MSPs are often found in binary systems, thus having high escape velocities from the gravitational potential wells in which they originated.

The observability of an extended bow-shock nebula structure depends on a variety of factors (Chatterjee & Cordes 2002; hereafter CC02). The surface brightness of a resolvable nebula, although a small fraction of the total energy output of the corresponding neutron star, will be proportional to $\dot{E}/D^2$, where D is the distance to the system in kpc. A limb-brightened structure is visible for higher values of the transverse velocity v_T. Higher values of the ambient interstellar medium (ISM) density n_H result in more energetic shocks; however, low ionization fractions are also required and consequently the radiative processes involved are primarily ram-pressure driven.

Understanding the ambient ISM near and around pulsars is important for studying the ambient density structure of the ISM in general. Variations in dispersion measure (DM), along with the presence of interstellar scattering and scintillation, all depend on the underlying structure of the ISM along the lines-of-sight (LOSs) to radio pulsars. These are some of the important factors influencing the timing accuracy of radio pulsars for their ability to detect gravitational waves (Cordes 2013; Stinebring 2013).

The *Hα* nebula around radio pulsar B2224+65, referred to as the "Guitar Nebula" (GN) is the most dynamic bow-

Received 4 JUN 2016 **Revised** 11 AUG 2016 **Accepted** 13 AUG 2016
†**Corresponding Author**
E-mail: tdolch@hillsdale.edu, ORCID: 0000-0001-8885-6388
Tel: +1-517-607-2449, Fax: +1-517-607-2206

shock system currently known. PSR B2224+65[1], an otherwise unremarkable canonical pulsar with period P ~ 0.68 sec and an $\dot{E}$ ~ 1.2×10^{33} erg/s, is amongst the highest velocity neutron stars known (v_T ~ 800-1,700 km/s; the uncertainty comes from the distance 1-1.9 kpc). The GN was discovered as part of a Palomar observatory survey of radio pulsars (Cordes et al. 1993), and the inclination angle close to 90° with respect to the LOS (CC02) means that any changing structures are maximally visible. The extremely high velocity is consistent with a natal velocity kick from an asymmetric supernova. A campaign of follow-up observations with the Palomar 200-inch Hale telescope, in conjunction with observations of the guitar head from the Hubble space telescope (HST), showed that the ambient ISM density decreased by a factor of about 30 %, from 0.006 to 0.004 cm^{-3}, for D = 1.9 kpc, over 7 yr (Chatterjee & Cordes 2004; hereafter CC04). These changes occurred over 1.3″, or ~2,500 AU. The expansion of the tip of the nebula was consistent with the radio proper motion measurement of 182 ± 3 mas/yr (Harrison et al. 1993; hereafter HLA93). In addition to density gradients, the time sequence of observations revealed inhomogeneities that constrained the ISM's density fluctuation power spectrum. NRAO very large array searches for nonthermal radio-synchrotron nebular structure resulted in non-detections (CC02). At X-ray energies, Chandra ACIS-S3 observations revealed an off-axis X-ray jet originating at the tip of the GN (Wong et al. 2003; Hui & Becker 2007). Hui et al. (2012), using XMM-Newton images, found X-ray flux near the pulsar, but no X-ray pulsations. No associated *Fermi*-LAT sources were found.

2. OBSERVATIONS

Motivated by the ~7 yr timescale of observed changes in the GN (CC04), we used Hα imaging at the 4.3 m Discovery Channel Telescope (DCT) at Lowell observatory to observe the GN, 22 yr after its original discovery. Using the large monolithic imager[2] (LMI) with its 12.5'×12.5' field of view (FOV), the DCT is extremely well-suited to image the largest length scales of the GN, enabling high-quality surface photometry down to 30 mag/arcsec^2 in the B and V bands.

Observations were taken on 24 Oct 2014 for 5 hr, with about 86 % of the time on the *Hα* ON filter (center wavelength 6,564.9 Å, bandwidth 30.1 Å) and the remaining time spent on the *Hα* OFF filter (center wavelength 6,459.1 Å, bandwidth 114.6 Å). Pixels were binned in 2×2 mode in order to reduce read noise, resulting in images with a 0.24″ pixel scale. Apart from some very light cloud cover, the seeing remained high-quality, reaching about 0.5″ toward the end of the night. We compare these images to those from the 1995 Palomar observations with the 200-inch Hale telescope and the 1994 HST images, both are described in CC02.

The pointings were combined using IRAF/PyRAF tasks. We obtained an ON DCT image (Fig. 1) after appropriate scaling. Then, using the geotran task in IRAF, we aligned the 1995 Palomar image (Fig. 2) with the ON DCT image and found the difference image (Fig. 3) after appropriate time and bandwidth scaling.

3. RESULTS

Fig. 3 shows the forward proper motion at the tip. The expansion around the edges of the bottom of the head is also apparent. Interestingly, the rounded body of the GN has also expanded, but the regions inside have not, suggesting a higher density toward the middle of the nebula, confining the shocked medium. Figs. 4-6 are the corresponding images to Figs. 1-3, zoomed in on the head, except for Fig. 4 which is the ON – OFF image with time and bandwidth scalings applied. The ON – OFF image removes one small background star from the head. The circled region in Fig. 4 shows possible new structures forming at the tip of the nebula, referred to here as "sub-structure." No

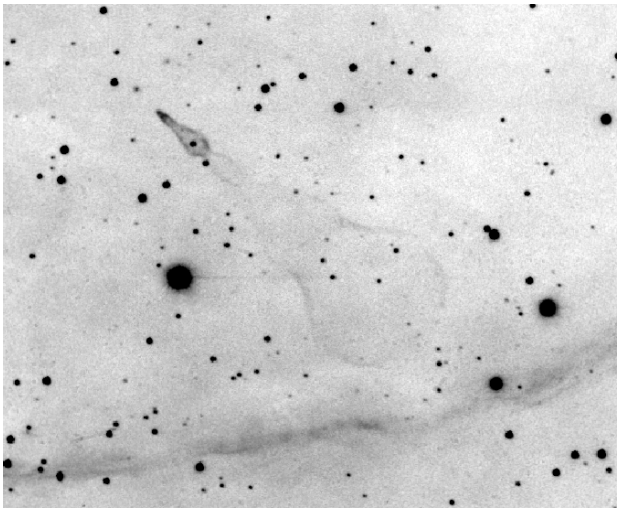

Fig. 1. *Ha* image of the Guitar Nebula (6,564.9 Å, bandwidth 30.1Å) taken with the 4.3 m Discovery Channel Telescope at Lowell observatory in late 2014. North is up, east is left. The colormap is inverted. The large horizontal filament is seen in the *Ha* image only and is not known to be related to the Guitar Nebula. The angular size of the image is about 2.5'×2'.

1 http://www.atnf.csiro.au/people/pulsar/psrcat/

2 http://www2.lowell.edu/users/massey/LMIdoc.pdf

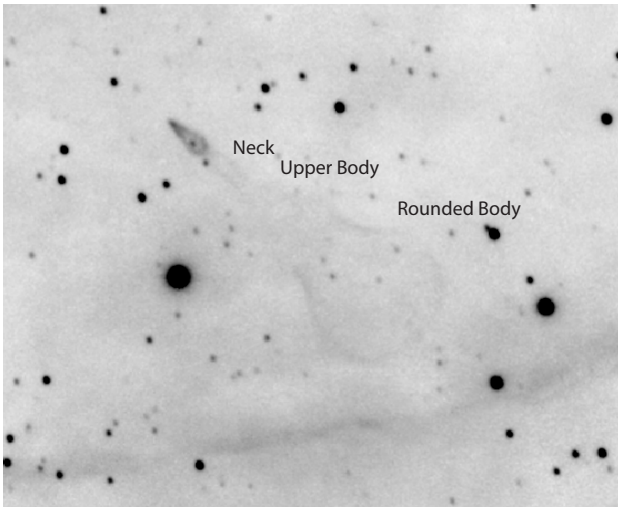

Fig. 2. *Ha* image of the Guitar Nebula (6,564 Å, bandwidth 20 Å) from the 5 m Hale telescope at Palomar observatory from 1995, described in CC02 and scaled and trimmed to match Fig. 1.

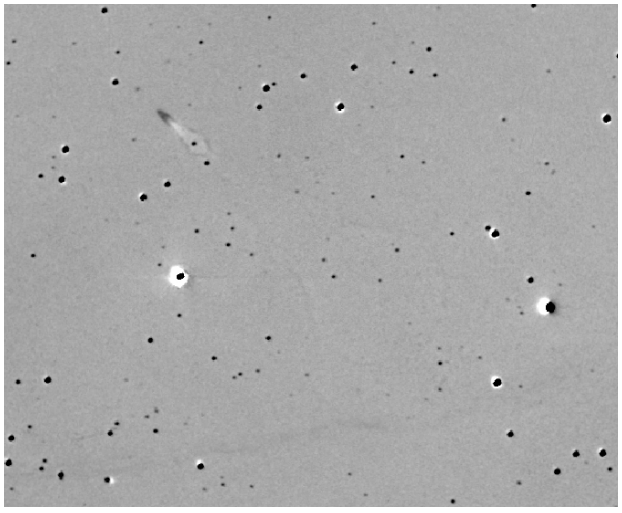

Fig. 3. Difference image of DCT minus Palomar images showing changes in the Guitar Nebula over the 19.3 yr between the observations. The rounded body has expanded at 0.05″/yr, but the upper body and neck have undergone little expansion.

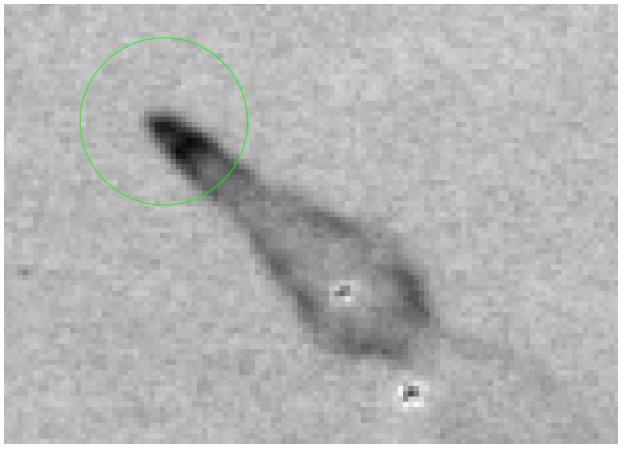

Fig. 4. *Ha* ON - OFF image of the Guitar Nebula (6,564 Å, bandwidth 20 Å ON; 6,459.1 Å, bandwidth 114.6 Å OFF) from the DCT. New substructure that may be forming in the tip is circled.

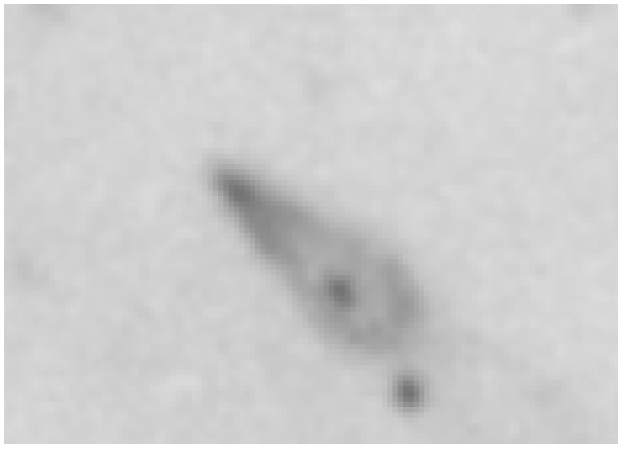

Fig. 5. *Ha* image of the Guitar Nebula head (6,564 Å, bandwidth 20 Å) from the 5 m Hale telescope at Palomar observatory from 1995, described in CC02. The cylindrical column between head and tip had not formed at the time these data were taken.

corresponding stars are visible at the same location in the tip of the OFF image. The limb-brightened edges of the GN head appear piecewise and disconnected, suggesting an inhomogeneous region.

In CC02, symmetric and antisymmetric images were obtained by mirroring the HST image of the GN head along the symmetry axis of the GN and taking the sum and difference, respectively. In the remaining analysis, we have used the ON image rather than the ON – OFF image because of the frequent comparisons to the 1995 Palomar image, which used an ON image only. We have performed a similar analysis in this paper and compared the results to those from the HST's wide field planetary camera 2 (WFPC2) in 1994. While the space-based WFPC2 data are obviously superior, especially given the detector's 0.0455″ pixel scale, it is interesting to note how closely the DCT-LMI image quality approaches that of HST images from the WFPC2 era.

Finding the GN's true position angle (PA) was not trivial. Observations of PSR B2224+65 with the Lovell telescope at Jodrell Bank observatory in HLA93 reported PA ~ 52.1° ± 0.9° while the bow-shock model that fits in CC02 reported PA ~ 48° ± 2°. One LMI pixel spans 1/225 of the GN's length. The minimum PA resolution available in these images is then ~0.25°. In order to find the effective PA for the DCT image of the GN head, we have performed a grid search in PA from 47° to 50° in steps of 0.25°, and for each angle, have created a rotated, repixelated image with the rotate task in IRAF and then have searched among 2–3 potential image columns for the axis

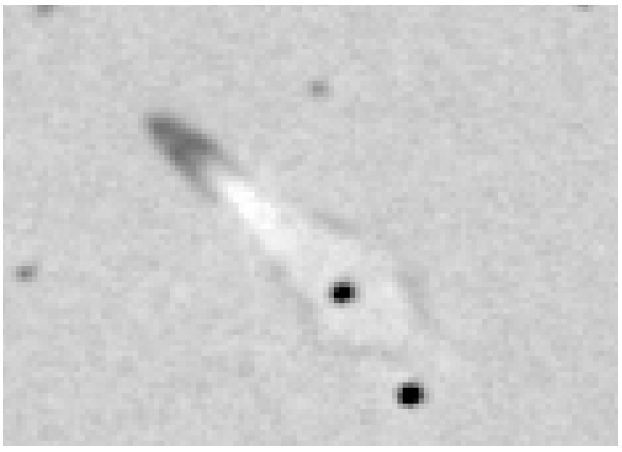

Fig. 6. Difference of DCT minus Palomar images showing changes in the Guitar Nebula head over the 19.3 yr between the observations. The pulsar has travelled at 0.18″/yr (Harrison et al. 1993), and the surface brightness has dimmed in the interior, especially immediately behind the tip. Asymmetric expansion has also occurred perpendicular to the pulsar's proper motion, near where the neck begins. The dark, expanded region at the tip spans ~3.4″. The radio pulsar is located at the furthest tip of the expanded region.

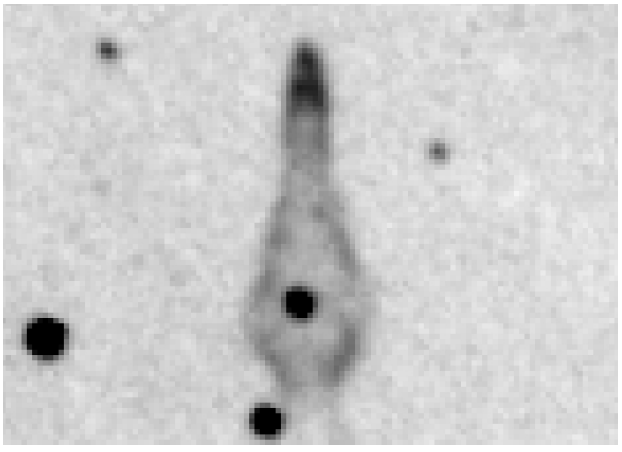

Fig. 7. DCT *Ha* ON image of the Guitar Nebula head, rotated by the nebula's effective position angle of 49.25°. In this view, the asymmetric, parallelogram-like structure of the limb-brightened edges becomes more apparent.

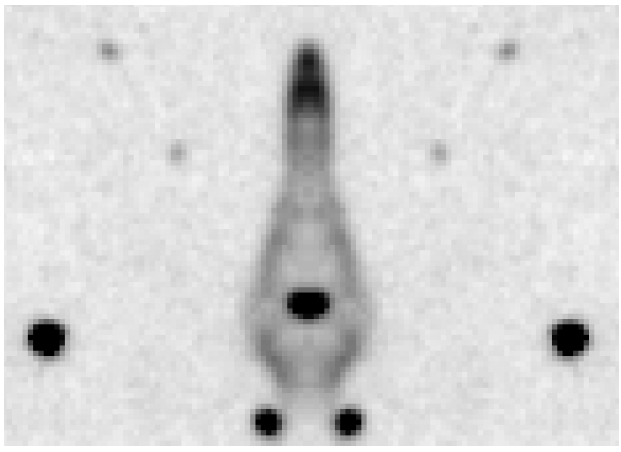

Fig. 8. Symmetric image of DCT *Ha* ON observation of the Guitar Nebula head, formed by mirroring the image along the symmetry axis and adding the images. The symmetric sub-structure at the tip becomes more pronounced. The head spans about 16″.

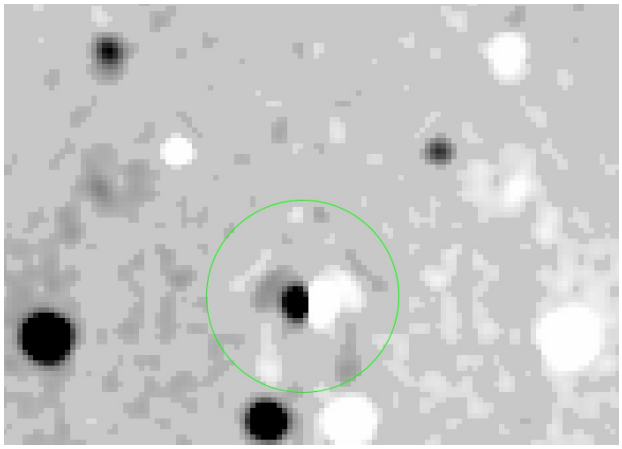

Fig. 9. Asymmetric image of the DCT *Ha* ON observation of the Guitar Nebula head. Each side is mirrored to the other, and the left – right difference images are computed and displayed. The resulting image is convolved with a Gaussian and noise is masked in order to emphasize the truly symmetric structures (see text for details). Asymmetries both in surface brightness and in spatial structure are apparent in the circled region, consistent with a density gradient in a direction different than the pulsar's proper motion. The star and its reflection in the center of the circle are 1.2″ apart. Within the green circle, the diagonal sets of parallel bright and dark lines represent the spatial asymmetries in limb structure, and the parallel vertical lines toward the bottom represent the surface brightness flux asymmetries. The symmetric surface brightness flux is a factor of 5 greater than the antisymmetric surface brightness flux. The absence of asymmetry as one approaches the tip (above the green circle) is apparent.

of symmetry that minimized the limb-brightened flux in the antisymmetric image. This process resulted in an effective PA of 49.25°, which we have used for the remaining analysis. While PA ~ 49.25° effectively minimizes the antisymmetric flux from the GN head, it does not minimize the antisymmetric flux from the GN body. However, there are parameters in the grid search for angles on each side of 49.25° that reduce the GN body's antisymmetric flux much more significantly than does the 49.25°-rotated image. It is not surprising that the GN body fails to constrain the PA well, owing to its larger angular scale and more diffuse structure. A highly symmetric tip, however, is predicted by bow-shock simulations (Wilkin 1996).

The resulting rotated, symmetric, and antisymmetric images are shown in Figs. 7-9 respectively. In the rotated image, the asymmetries at the bottom of the GN head are more apparent than in, for example, Fig. 4. The symmetric image (Fig. 8) highlights the same sub-structure at the GN tip shown in Fig. 4. The antisymmetric image (Fig. 9), following CC02, was computed by blurring with a Gaussian kernel, and zero-masking based on how the convolved image compared to the unconvolved noise. The original

difference image was convolved with a 1-pixel Gaussian, and pixel absolute values <1σ were zeroed, where σ is the image noise level, defined as the 10 sigma-clipped standard deviation of the original rotated image (Fig. 7).

In the circled region of Fig. 9, a number of interesting features are apparent. The parallel diagonal bands clearly show the asymmetric limb-brightened areas toward the bottom of the GN head. Such a radical spatial asymmetry was not present in the CC02 1994 HST images, in which the head asymmetry was primarily an asymmetry in the surface brightness of the limbs. Furthermore, the bottom of the head (toward the bottom of the marking circle) now appears to show a surface brightness asymmetry. As concluded in CC02, the surface brightness asymmetry is likely indicative of an ISM density gradient in a different direction than the neutron star's motion. More recently, however, this surface brightness asymmetry seems to have become present at the bottom of the head, and not on the limb-brightened edges only immediately behind the tip. Averaging over a number of corresponding pixels in the surface brightness asymmetry, we found that the ratio of antisymmetric surface brightness to the symmetric surface brightness is ~0.2. The spatially asymmetric structure requires a more complex model from which to draw further conclusions.

To estimate the forward motion at the tip, we took the central few columns of the difference image (Fig. 3) along the symmetry axis and sum them in the direction perpendicular to the symmetry axis. The sky location where the resulting column values cross zero represents the beginning of the tip motion tracked since 1995. On the positive side of this column, we used the maximum value as the fiducial 1995 tip position. The positive side of the column gradually drops toward the noise and we used the sky location for which the column value is equal to 1σ above the difference image's sky noise (outside the GN tip) as the fiducial current tip position. The difference in these pixel positions implies 170 ± 20 mas/yr over the 19.33 yr between images, which is within the uncertainties of the radio pulsar's motion from timing data. (The uncertainty assumes a 1-pixel error for the start and end of the expansion region in the difference image.)

Similarly, we estimated the expansion rate of the GN body by selecting one long, rectangular slice of positive-negative parallel limb arcs indicating outward expansion. For this small region in which the limbs are barely curved, we sum along the long direction to obtain a 1-D vector with a peak and a trough. The width of the positive region that rises 3σ above the surrounding noise outside the GN altogether is about four pixels. This is equivalent to an expansion rate of 50 ± 10 mas/yr for the GN body, or 200-500 km/s, assuming the 1-1.9 kpc distance range.

4. CONCLUSIONS AND FURTHER WORK

The changes in the GN since 1995, as recently imaged by the DCT, imply a 0.17″/yr proper motion at the tip, or about 0.7-1.1 % of c, which is highly supersonic for any phase of the ISM, and therefore a strong shock. The GN body expands at about 0.05″/yr. In the GN head, asymmetries in both limb-brightened spatial structure and in surface brightness appear to have occurred. Most intriguingly, additional sub-structure near the tip might have appeared. CC04 suggests that the head of the GN may be a second "guitar" undergoing formation due to confinement of the NS wind. Should a new structure at the tip represent a dense region of the ISM, it may be the beginning of a third "guitar."

The GN's evolution between 1995 and 2014 supports the model of the GN as a series of expanding bubbles through an HI ISM with varying density. The density variations are likely sufficient to explain the asymmetries and the time-varying structures in the limb-brightened regions. However, the structure of a bow-shock nebula is dependent on factors in addition to n_{H}, namely $\dot{E}$ and the ionization fraction of the surrounding medium. While Ockham's razor would seem to favor a varying n_H, it is intriguing to consider variations in $\dot{E}$, which could in principle correspond to timing glitches in PSR B2224+65, a number of which have been reported (Janssen & Stappers 2006; Yuan et al. 2010). Continued radio monitoring could therefore be used to test for $H\alpha$ structure changes in correlation with glitch events. Also, a changing ionization fraction, or lack thereof, could be deduced from a DM monitoring campaign on the pulsar. Properties of the associated X-ray filament may also change on dynamic timescales, and would benefit from a periodic observing campaign with Chandra and/or Newton-XMM.

ACKNOWLEDGMENTS

Shami Chatterjee, James M. Cordes, and Timothy Dolch were partially supported through the National Science Foundation (NSF) PIRE program award number 0968296. Dan P. Clemens and Lauren R. Cashmen acknowledge support from the NSF under AST09-07790 and AST14-12269. Timothy Dolch also thanks the Douglas R. Eisenstein research gift to Hillsdale college. These results made use of the Discovery Channel Telescope at Lowell observatory, supported by Discovery Communications, Inc., Boston University, the University of Maryland, the University of Toledo and Northern Arizona University. PyRAF is a product of the Space Telescope Science Institute, which is operated by AURA for NASA. This research has made use of NASA's Astrophysics Data System.

REFERENCES

Brownsberger S, Romani RW, A survey for *Hα* pulsar bow shocks, Astrophys. J. 784, 154-167 (2014). http://dx.doi.org/10.1088/0004-637X/784/2/154

Chatterjee S, Cordes JM, Bow shocks from neutron stars: scaling laws and *Hubble space telescope* observations of the Guitar nebula, Astrophys. J. 575, 407-418 (2002). http://dx.doi.org/10.1086/341139

Chatterjee S, Cordes JM, Smashing the Guitar: an evolving neutron star bow shock, Astrophys. J. Lett. 600, L51-L54 (2004). http://dx.doi.org/10.1086/381498

Cordes JM, Limits to PTA sensitivity: spin stability and arrival time precision of millisecond pulsars, Class. Quantum Grav. 30, 224002 (2013). http://dx.doi.org/10.1088/0264-9381/30/22/224002

Cordes JM, Romani RW, Lundgren SC, The Guitar nebula: a bow shock from a slow-spin, high-velocity neutron star, Nature 362, 133-135 (1993). http://dx.doi.org/10.1038/362133a0

Harrison PA, Lyne AG, Anderson B, New determinations of the proper motions of 44 pulsars, Mon. Not. Roy. Astron. Soc. 261, 113-124 (1993). http://dx.doi.org/10.1093/mnras/261.1.113

Hui CY, Becker W, X-ray emission properties of the old pulsar PSR B2224+65, Astron. Astrophys. 467, 1209-1214 (2007). http://dx.doi.org/10.1051/0004-6361:20066562

Hui CY, Huang RHH, Trepl L, Tetzlaff N, Takata J, et al., XMM-newton observation of PSR B2224+65 and its jet, Astrophys. J. 747, 74-85 (2012). http://dx.doi.org/10.1088/0004-637X/747/1/74

Janssen GH, Stappers BW, 30 glitches in slow pulsars, Astron. Astrophys. 457, 611-618 (2006). http://dx.doi.org/10.1051/0004-6361:20065267

Romani RW, Shaw MS, Camilo F, Cotter G, Sivakoff GR, The Balmer-dominated bow shock and wind nebula structure of γ-ray pulsar PSR J1741-2054, Astrophys. J. 724, 908-914 (2010). http://dx.doi.org/10.1088/0004-637X/724/2/908

Stinebring D, Effects of the interstellar medium on detection of low-frequency gravitational waves, Class. Quantum Grav. 30, 224006 (2013). http://dx.doi.org/10.1088/0264-9381/30/22/224006

Wilkin FP, Exact analytic solutions for stellar wind bow shocks, Astrophys. J. Lett. 459, L31-L34 (1996). http://dx.doi.org/10.1086/309939

Wong DS, Cordes JM, Chatterjee S, Zweibel EG, Finley JP, et al., Chandra observations of the Guitar nebula, Proceedings of the 214th Symposium of the International Astronomical Union (IAU), Suzhou, China, 6-10 August 2003.

Yuan JP, Wang N, Manchester RN, Liu ZY, 29 glitches detected at Urumqi observatory, Mon. Not. Roy. Astron. Soc. 404, 289-304 (2010). http://dx.doi.org/10.1111/j.1365-2966.2010.16272.x